The cycle-to-cycle variability of Cygnus X-3

van der Klis, M.B.M.; Bonnet-Bidaud, J.M.

Published in:
Astronomy and Astrophysics Supplement Series

ASTRONOMY & ASTROPHYSICS
SUPPLEMENT SERIES

Astron. Astrophys. Suppl. Ser. **50**, 129-140 (1982)

The cycle-to-cycle variability of Cygnus X-3

M. van der Klis (*) (**) and J. M. Bonnet-Bidaud (***)

(*) Astronomical Institute, University of Amsterdam, Roetersstraat 15, 1018 WB Amsterdam, The Netherlands.
(**) Cosmic Ray Working Group, Leiden, The Netherlands.
(***) CEN Saclay, DPh-EP/SAp, 91191 Gif-sur-Yvette Cedex, France

Received October 22, accepted April 30, 1982

Summary. — Results are reported of a study of the variability of the shape of the light curve of Cyg X-3 from one cycle to the next on time scales down to ~ 200 s. Variations occur mainly around the maximum of the light curve, on a time scale of about half an hour or less, and give rise to a dispersion of the individual light curves around the mean which is a considerable fraction of the amplitude of the modulation.

Key words : X-ray binaries — Cygnus X-3.

1. **Introduction.** — The smooth 0.2 d modulation of the X-ray flux of Cyg X-3 could be due to scattering of the X-rays in a structure at least the size of the binary orbit (Pringle, 1974 ; Davidsen and Ostriker, 1974 ; Milgrom, 1976), or to partial occultation of an extended X-ray source (i.e. a shock front, Bignami *et al.*, 1977 ; or a disk corona, White and Holt, 1982). X-ray variability on shorter time scales than the orbital period could be expected to contain information on properties of the system on a scale small compared to the binary separation. This cycle-to-cycle variability, which is left largely unexplained in any theory on the modulation of Cyg X-3, was noticeable in data obtained with the Copernicus (Mason *et al.*, 1976) and Uhuru and ANS satellites (Parsignault *et al.*, 1977).

Due to their long duration (~ 127 d), the pointed COS-B observations of Cyg X-3 are particularly useful for the study of an unpredictable phenomenon like this short term variability. We present in this paper examples of light curve trains, which demonstrate the various aspects of the variability of Cyg X-3 on time scales less than the orbital period down to ~ 200 s ; we were also able to perform a statistical study of the variability of the cycle-to-cycle variability itself.

The behaviour of the source on longer time scales has already been reported in Paper 1 (Bonnet-Bidaud and van der Klis, 1981).

2. **Observations.** — Figure 1 shows the mean counting rate obtained with the 80 cm^2 (2-12 keV) X-ray detector onboard the COS-B satellite, during three separate pointings of Cyg X-3 in 1977, 1978 and 1980. Data obtained in each one-month observation are shown at the same scale after background subtraction and correction for the satellite attitude. The ~ 24 h blocks of data in figure 1 correspond to the useful part of the 36 h satellite orbit ; the gaps are due to data rejection because of the passage of the satellite through the radiation belts of the earth and in some cases to high particle contamination (for a full description of the satellite and data, see Paper 1). The source flux in figure 1 has been averaged over ~ 0.5 h intervals, showing clearly the individual 4.8 h cycles of the source as well as the changes of the mean level and the amplitude of the modulation (1 COS-B c/s $\simeq$ 2.3 to 2.7 $\times$ 10^{-10} erg cm^{-2} s^{-1} for the range of spectra given for Cyg X-3 by Mason *et al.*, 1976 and Becker *et al.*, 1978).

To allow a direct comparison of the different cycles in spite of these changes, the flux in each satellite orbit interval was normalized. A sine fit was performed in each interval and the flux was corrected according to the prescription : normalized flux = (flux-A_0)/A_1, where A_0 and A_1 are, respectively, the mean level and the amplitude determined from the fit. The time extent and the normalization constants for each interval are listed in table I.

Figure 2 shows some of these normalized cycles plotted at an identical ordinate scale with a resolution of ~ 200 s (twice the full resolution of the instrument). They were selected to be representative of the different observed intensity levels of the source, and are identified in figure 1. The signal-to-noise ratio in 1977 and 1978 was smaller than in 1980 due to less favourable pointing directions and source intensities ; therefore the lowest intensity parts of these observations are not presented.

Data obtained in the three different years show a similar degree of variability, which is characterized by :

— a considerable change in the shape of the modulation from cycle to cycle. This change could either look

gradual (see X_3 and I_3) or erratic (E_1, G_1 and O_3). In some cases the cycle shape stays rather stable (see R_3 and U_3), but from all inspected cycles this was found to be the case only in the higher intensity part of 1980 ;

— the absence of any phase-stable feature ;

— the presence of flux enhancements on time scales of the order of 0.5 h. This was observed previously in Copernicus data (Mason *et al.*, 1976). From all cycles obtained, such features were only seen in the phase interval 0.2-0.8 (see E_1, G_1, B_2 and O_3).

3. **Analysis.** — In order to quantify the above described light curve variability and to study its dependence on orbital phase, we have employed a folding technique. Segments of the, background and aspect corrected, data, selected according to intensity level were binned into 0.01 cycle phase bins, according to the ephemeris of van der Klis and Bonnet-Bidaud (1981). Table I gives the limits of the chosen segments, which cover all the available data. The variances of the fluxes accumulated in each bin were then computed as a measure of the dispersion.

If this technique is applied to unnormalized counting rates, dispersion curves are obtained which closely resemble the light curve, due to the dominant and near-proportional variation of the amplitude and the mean level of the modulation. Once normalized as described above, the dispersion of the signal will mainly be due to statistics and to cycle-to-cycle variability.

The quantities plotted in figure 3 are the variance $\sum_i (f_i - \bar{f})^2/(n-1)$ (upper curves) of the n normalized fluxes f_i accumulated in one phase bin, and the dispersion which would have been expected purely on the basis of counting statistics $\sum_i \sigma_i^2/n$, where σ_i is the statistical uncertainty, from Poisson statistics, of f_i after background subtraction, aspect correction and normalization (lower curves). The difference between these curves is a measure of the intrinsic variability of the modulation as a function of orbital phase. The ordinate of the figures is expressed as a fraction of the amplitude of the modulation, A_1.

There are several effects which could bias the dispersion curves obtained in this way :

— Satellite aspect uncertainties. The relative accuracy of the satellite pointing direction reconstruction is 0.05° (Boella *et al.*, 1974). This corresponds to a relative angular detector efficiency change of 1 % when observing at 50 % efficiency, and could lead to an extra dispersion of 1 % of the total signal, or up to about $3 \times 10^{-4} A_1^2$ in variance.

— The uncertainties introduced in the normalization procedure. The formal uncertainties in A_1 and A_0 are usually a few percent (see Table I), and would give rise to variances of the order of $0.01\ A_1^2$. They have been ignored for the purpose of the calculation of the expected dispersions.

— Phase shifts of the 4.8 h cycle. These are observed to be of the order of 0.01 cycle (Paper 1) and would not contribute more than $0.01\ A_1^2$ to the dispersion even in the steepest part of the light curve.

— The effect of mean flux and amplitude variations which were not removed by the normalization procedure. This effect is not directly distinguishable from the light curve variability itself. The variations of A_0 and A_1 visible in the normalized data (now defined as the mean, and the difference of the maximum and the minimum of the individual light curve, respectively), are of the same order as the observed dispersion. The fact that the dispersion curves do not, in most cases, mimic the Cyg X-3 light curve, shows that these variations are indeed mainly due to cycle-to-cycle variability.

It is clear from the obtained dispersion curves that the distribution of the variability of the light curves over orbital phase is variable and sometimes quite complex (see 1980 I to V), although in general the region around the minimum of the light curves (0.8-1.2) is found to be less variable than the remaining part.

We also computed an analogous quantity, the percentage rms fluctuations of the unnormalized signal, according to the method described by Parsignault *et al.* (1977). Contrary to their results, at the signal-to-noise level of the COS-B data, these fluctuations are clearly dependent on orbital phase.

The phase dependence of the dispersion was also calculated on a 24 h time scale. Table I gives the ratio of the dispersion in the intervals $\phi = 0.1325$-0.6875 (maximum) and $\phi = 0.8438$-1.1250 (minimum) to the mean counting statistics dispersion for each satellite orbit. In three out of every four cases, the dispersion around the maximum of the light curve is larger than around the minimum.

In an attempt to obtain more information about the time scales of the variability, we calculated the power spectra and the autocorrelation functions of each of the one month observations. The power spectra revealed no statistically significant coherent pulsations in the time scale range of a few days down to ~ 200 s, except, of course, for the 4.8 h modulation and its harmonics.

The 4.8 h modulation is the dominant feature in the autocorrelation function (ACF) (Fig. 4). The contribution of short time scale fluctuations to the ACF can be estimated, however, on the assumption that the secondary maxima due to the correlation of the individual light curves with their direct neighbours differ only from the primary maximum because of two effects :

— the data gaps (see Fig. 1), causing a general downward trend towards larger delay, slightly asymmetrizing the secondary peaks, and ;

— the short time scale intensity fluctuations, effectuating an enhancement of the ACF near zero delay in addition to the sharp peak caused by the statistical noise.

Replotting the secondary maxima to a somewhat (30-40 %) extended vertical scale to give them the same amplitude as the primary maximum, it was found on superposing the curves (dotted lines in Fig. 4), that they coincide nearly completely, except in the minima, where the asymmetry of the secondary maxima becomes dominant, and around maximum. The latter discrepancy, amounting to $(0.05$-$0.10)\ A_1$, is interpreted as the effect

of the short term intensity fluctuations, which are thus estimated to occur on time scales below ~ 3 000 s. Variations in the pointing direction of the instrument on these time scales are damped to less than 1′ within a few minutes after the acquisition of the target and are thus many orders of magnitude below the amplitude required to explain the observed fluctuations from satellite aspect variability. It is therefore concluded, that Cyg X-3 shows fluctuations in X-ray intensity on typical time scales of a few thousand seconds and less, with an amplitude of 5-10 % of the 4.8 h modulation.

4. **Conclusion.** — The variability of the 4.8 h light curve from cycle to cycle seems to be unconnected to the systematic variations of the mean shape of the light curve (see also Paper 1) and to the long term intensity changes. Its time scale, of the order of a few thousand seconds, corresponds to free fall times at around the orbital radius of the binary.

In the picture of a close binary surrounded by a large scale structure of scattering gas, there is a natural division between the long term variations due to changes in this large scale structure, and the cycle-to-cycle variability, originating in fluctuations in X-ray emission or absorption close to the compact object. The lower intrinsic variability of the minimum of the light curve then finds an explanation in eclipses of the X-ray source by the companion star (see also Paper 1).

In a partial occultation model one would have to explain not only the short term fluctuations, but also the systematic light curve changes, in terms of variations in the X-ray source and the occulting body, both of similar, relatively small ($\lesssim 10^{11}$ cm) size.

Acknowledgements. — The authors would like to thank the referee for pointing out several possible concerns about the significance of the observed dispersions and the possible influence of systematic effects such as satellite drift. MVD K aknowledges support from the Netherlands Organisation for the Advancement of Pure Research ZWO (ASTRON).

References

BECKER, R., ROBINSON-SABA, J., BOLDT, E., HOLT, S., PRAVDO, S., SERLEMITSOS, P. and SWANK, J. : 1978, *Astrophys. J. Lett.* **224,** L113.
BIGNAMI, G., MARASCHI, L. and TREVES, A. : 1977, *Astron. Astrophys.* **51,** 512.
BOELLA, G., BUCCHERI, R., BURGER, J., COFFARO, P. and PAUL, J. : 1974, *Proc. 9th ESLAB Symp. ESRO SP-106,* 345.
BONNET-BIDAUD, J. M. and VAN DER KLIS, M. : 1981, *Astron. Astrophys.* **101,** 299.
DAVIDSEN, A. and OSTRIKER, J. : 1974, *Astrophys. J.* **189,** 331.
MASON, K., SANFORD, P. and IVES, J. : 1976, *in « X-ray binaries »* (Goddard), NASA SP-389, p. 255.
MILGROM, M. : 1976, *Astron. Astrophys.* **51,** 512.
PARSIGNAULT, D., GRINDLAY, J., GURSKY, H. and TUCKER, W. : 1977, *Astrophys. J.* **218,** 232.
PRINGLE, J. : 1974, *Nature* **247,** 21.
VAN DER KLIS, M. and BONNET-BIDAUD, J. M. : 1981, *Astron. Astrophys.* **95,** L5.
WHITE, N. E. and HOLT, S. S. : 1982, *Astrophys. J.* (to be published).

TABLE I. — *Characteristics of the 4.8 h modulation during the 24 h useful part of each of the satellite orbits. TSTART and TEND are the start and the end time of the data stretch in JD-2443282.5. A0 and A1 are the mean level and the amplitude of the modulation as derived from a sine fit to the data, respectively ; SIGA0 and SIGA1 are their one-parameter one sigma uncertainties. DMAX, DMIN and DE are, respectively, the dispersion of the maximum and the minimum of the light curves and the phase averaged dispersion expected from counting statistics (see text). These quantities are all in c/s. The data segments used for figure 3 are indicated at right.*

INTERVAL	TSTART	TEND	A0	SIGA0	A1	SIGA1	DMAX/DE	DMIN/DE	DE	
A1	20.46	21.24	18.74	0.18	6.31	0.25	1.07	1.09	4.33	
B1	21.64	22.74	18.62	0.17	5.42	0.23	1.08	1.08	4.34	
C1	23.11	24.09	20.42	0.20	6.24	0.29	1.45	1.24	4.36	H
D1	24.64	25.79	25.43	0.19	10.41	0.26	1.40	1.19	4.41	H
E1	26.23	27.34	27.95	0.17	10.61	0.24	1.35	1.06	4.44	H
F1	27.82	28.90	27.91	0.21	10.63	0.28	1.64	1.21	4.46	H
G1	29.23	30.31	23.97	0.18	7.68	0.25	1.56	1.08	4.35	H
H1	30.86	31.51	19.56	0.19	5.72	0.26	1.04	1.14	4.32	L
I1	32.29	33.29	13.56	0.15	3.53	0.21	1.04	1.02	4.23	L
J1	33.85	34.66	14.38	0.19	4.10	0.27	1.18	1.11	4.27	L
K1	35.40	36.38	12.88	0.16	3.32	0.22	1.10	1.13	4.23	L
L1	37.01	38.06	12.87	0.16	3.53	0.22	1.16	1.00	4.26	L
M1	38.41	39.50	13.27	0.17	3.12	0.23	1.05	1.25	4.32	L
N1	39.98	41.12	13.28	0.15	3.76	0.21	0.93	1.06	4.30	L
O1	41.46	42.52	15.91	0.17	3.96	0.24	1.29	1.10	4.29	L
P1	43.01	44.19	19.13	0.18	5.53	0.25	1.24	1.23	4.28	L
Q1	44.57	45.63	16.43	0.17	5.13	0.23	1.24	1.04	4.25	L
R1	46.18	47.09	14.19	0.15	3.36	0.22	1.00	1.17	4.21	L
S1	47.58	48.75	16.78	0.18	4.76	0.26	1.21	1.22	4.31	L
T1	49.16	50.21	18.71	0.16	6.64	0.23	1.26	1.02	4.32	L
U1	50.66	51.83	16.12	0.16	4.25	0.23	1.10	1.05	4.30	L
V1	52.18	53.20	17.19	0.17	5.34	0.24	1.24	1.02	4.32	L
W1	53.75	54.89	18.35	0.17	5.08	0.24	1.12	1.09	4.34	L
X1	55.36	56.37	19.49	0.23	4.78	0.34	1.17	1.28	4.40	L
Y1	55.76	57.44	18.88	0.21	7.05	0.28	1.15	1.10	4.43	L

CYGNUS X-3 - NOV./DEC. 1978

INTERVAL	TSTART	TEND	A0	SIGA0	A1	SIGA1	DMAX/DE	DMIN/DE	DE	
A2	534.09	534.87	23.51	0.27	8.07	0.38	1.48	1.06	4.48	H
B2	535.67	536.64	27.30	0.22	10.38	0.31	1.57	1.24	4.55	H
C2	537.12	538.22	27.31	0.20	6.82	0.28	1.12	1.06	4.60	H
D2	538.70	539.72	20.96	0.18	5.26	0.24	1.14	1.04	4.61	H
F2	543.46	543.64	*****	****	*****	****	****	****	****	
G2	544.82	545.39	10.32	0.20	3.64	0.27	1.10	1.02	4.49	L
H2	546.29	547.37	10.92	0.17	3.05	0.25	1.09	1.11	4.47	L
I2	547.84	548.77	10.94	0.19	2.81	0.26	1.05	1.05	4.50	L
J2	549.41	550.46	11.14	0.17	3.39	0.24	1.12	1.12	4.48	L
K2	551.01	551.22	7.81	0.27	2.60	0.37	1.11	0.73	4.47	L
L2	552.44	553.41	9.01	0.18	3.23	0.26	1.12	1.12	4.39	L
M2	553.98	554.80	7.94	0.22	2.18	0.30	1.04	1.20	4.38	L
N2	555.50	556.52	7.40	0.18	1.41	0.25	1.03	1.06	4.33	L
O2	556.99	557.43	6.85	0.24	2.69	0.33	1.10	1.15	4.34	L
P2	558.65	558.98	8.18	0.25	2.65	0.33	1.00	0.86	4.46	L
Q2	560.21	560.87	9.36	0.23	2.23	0.32	1.10	1.13	4.53	L
R2	561.63	562.64	9.86	0.18	2.72	0.25	1.06	1.10	4.59	L
S2	563.59	564.18	10.62	0.23	2.46	0.34	1.06	1.09	4.58	L
T2	567.78	568.69	12.50	0.20	2.83	0.28	1.13	1.11	4.60	L
U2	569.34	569.71	11.57	0.25	2.02	0.38	1.16	1.02	4.58	L
V2	570.78	571.35	15.59	0.28	1.25	0.37	1.13	1.34	4.66	L

CYGNUS X-3 - MAY/JUNE 1980

INTERVAL	TSTART	TEND	A0	SIGA0	A1	SIGA1	DMAX/DE	DMIN/DE	DE	
A3	1091.37	1091.80	13.34	0.13	4.01	0.18	1.25	1.39	2.01	I
B3	1092.43	1093.28	12.94	0.09	3.62	0.13	1.29	1.12	2.01	I
C3	1093.90	1094.95	13.40	0.08	3.72	0.11	1.20	1.05	2.01	I
D3	1095.39	1096.30	14.27	0.09	4.02	0.12	1.37	0.98	2.05	I
E3	1097.00	1098.01	16.85	0.09	5.44	0.12	1.27	1.03	2.08	I
F3	1098.57	1098.94	22.26	0.13	7.14	0.17	1.24	0.89	2.13	II
G3	1100.00	1101.03	23.52	0.11	9.44	0.16	1.89	1.23	2.18	II
H3	1101.54	1102.35	24.85	0.12	7.74	0.17	1.40	1.11	2.19	II
I3	1103.36	1104.13	30.95	0.11	11.58	0.17	1.81	1.14	2.24	II
J3	1105.14	1105.41	26.82	0.17	6.84	0.24	1.00	1.43	2.22	II
K3	1107.72	1108.63	29.15	0.13	10.04	0.17	2.20	1.29	2.27	III
L3	1109.18	1110.19	32.59	0.14	11.50	0.20	2.02	1.49	2.27	III
M3	1110.70	1111.78	27.68	0.12	10.15	0.16	1.74	1.38	2.23	III
N3	1112.25	1113.21	30.57	0.13	14.20	0.17	2.50	1.31	2.27	III
O3	1113.76	1114.82	31.80	0.13	12.70	0.17	2.58	1.19	2.30	III
P3	1115.50	1116.23	41.45	0.15	17.85	0.22	1.95	1.36	2.52	IV
Q3	1116.97	1117.87	38.08	0.16	18.79	0.20	1.91	1.68	2.33	IV
R3	1118.33	1119.25	43.40	0.13	19.04	0.18	1.80	1.26	2.33	IV
S3	1119.94	1120.96	39.10	0.14	16.76	0.18	1.75	1.45	2.32	IV
T3	1121.53	1122.27	43.05	0.18	20.32	0.22	2.07	1.61	2.37	IV
U3	1123.15	1124.02	47.90	0.15	18.73	0.22	1.95	1.50	2.48	V
V3	1124.70	1125.29	45.27	0.21	20.91	0.26	2.75	1.31	2.49	V
W3	1126.28	1127.07	51.08	0.15	22.04	0.20	2.11	1.08	2.63	V
X3	1127.66	1128.32	41.22	0.17	17.96	0.22	2.92	1.14	2.54	V
Z3	1130.68	1131.60	43.19	0.18	12.34	0.25	1.92	1.37	3.14	V

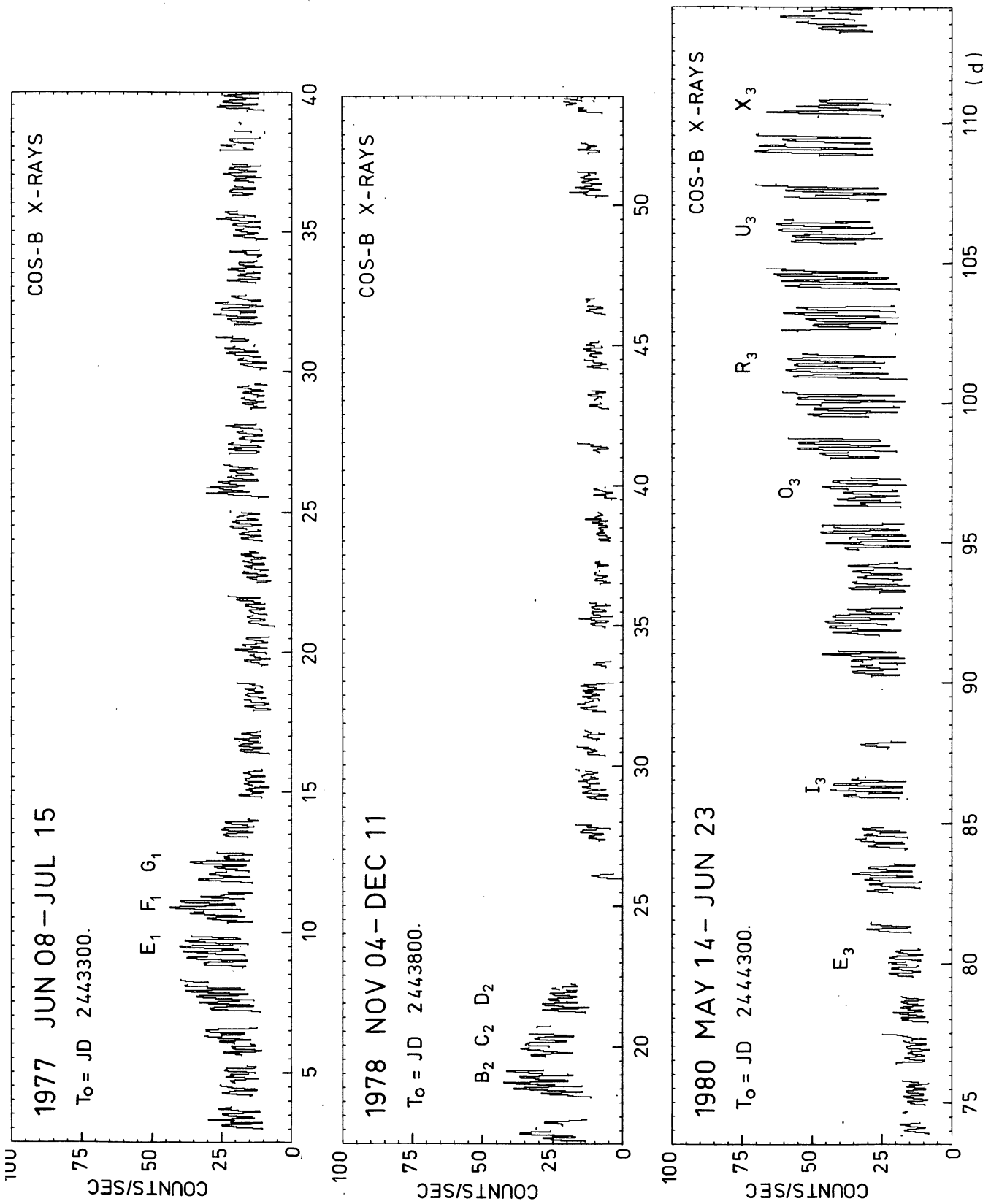

FIGURE 1. — A summary of the observations at a resolution of about 0.5 h. Statistical errors are less than 1 c/s (1σ). Data gaps are due to passage of the satellite through the radiation belts of the earth. About 5 cycles of the 4.8 h modulation are visible in each contiguous data block. Identified data blocks are given at full resolution in figure 2.

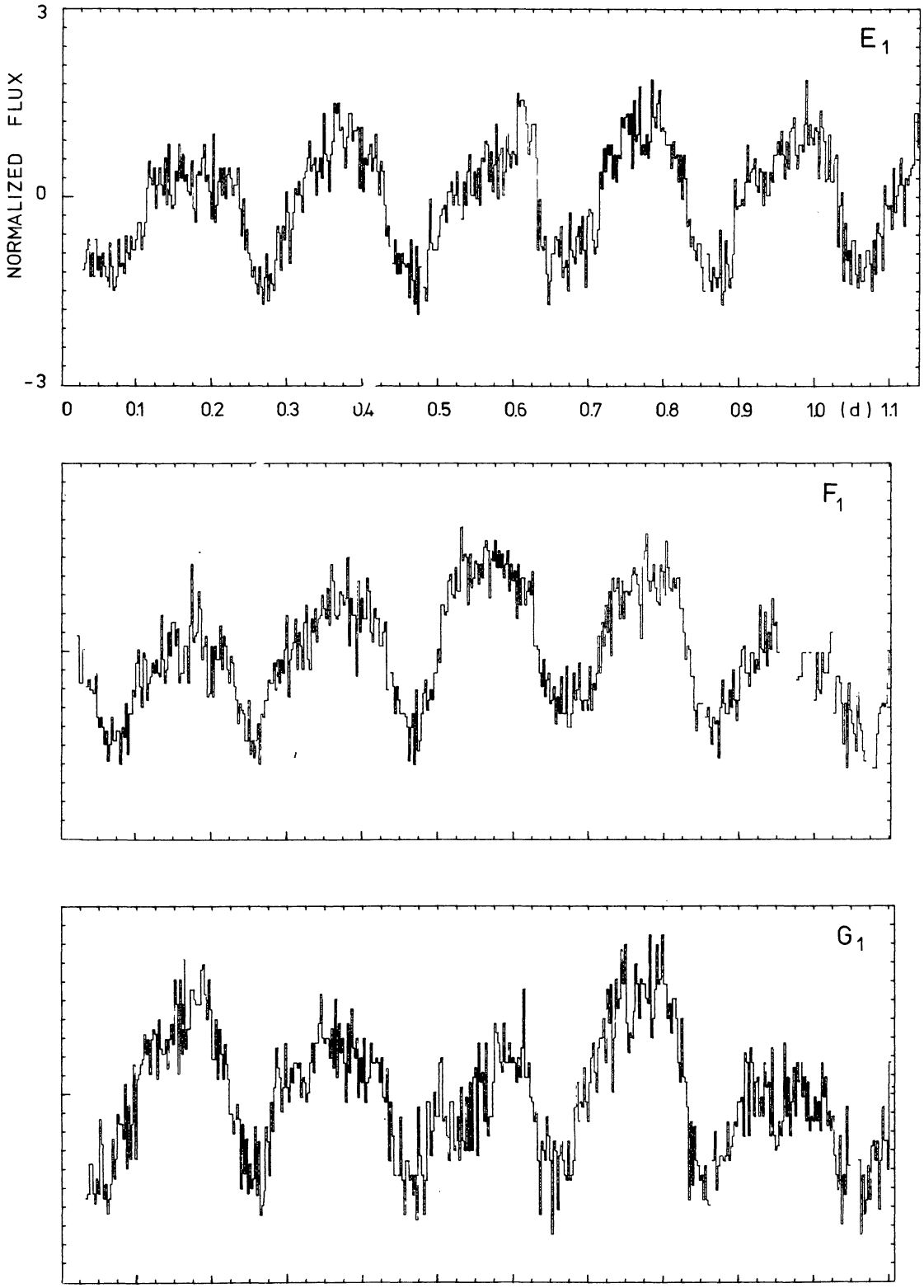

FIGURE 2*a*

FIGURE 2. — A selected set of light curve trains at a resolution of ~ 200 s, normalized to show the same amplitude (see text). Statistical error per bin varies from 10 % (R_1) to 50 % (D_2) of the amplitude, depending on the level of the source and its position in the field of the detector. Data trains are identified in figure 1. All scales are as in first frame.

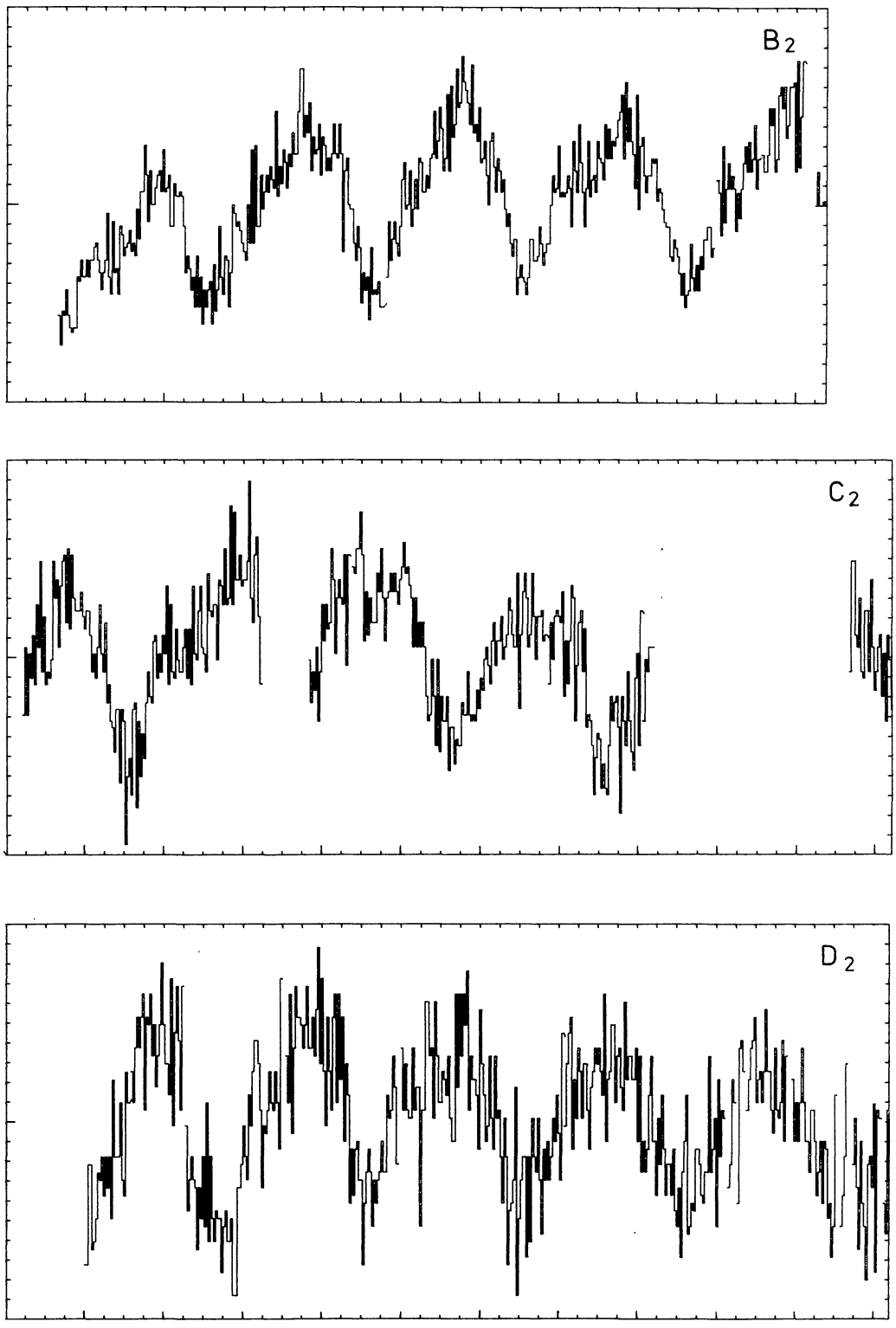

FIGURE 2*b*

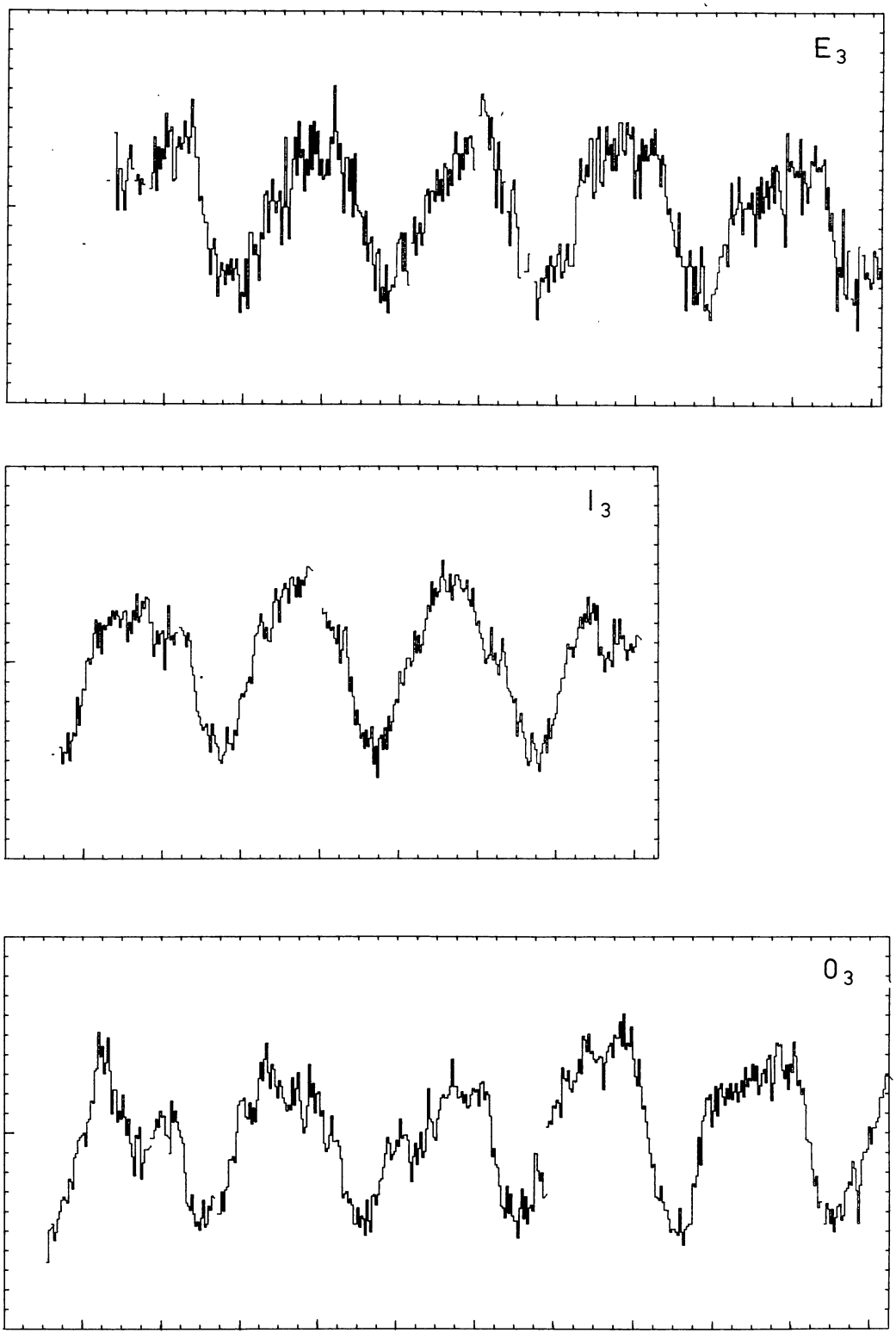

FIGURE 2*c*

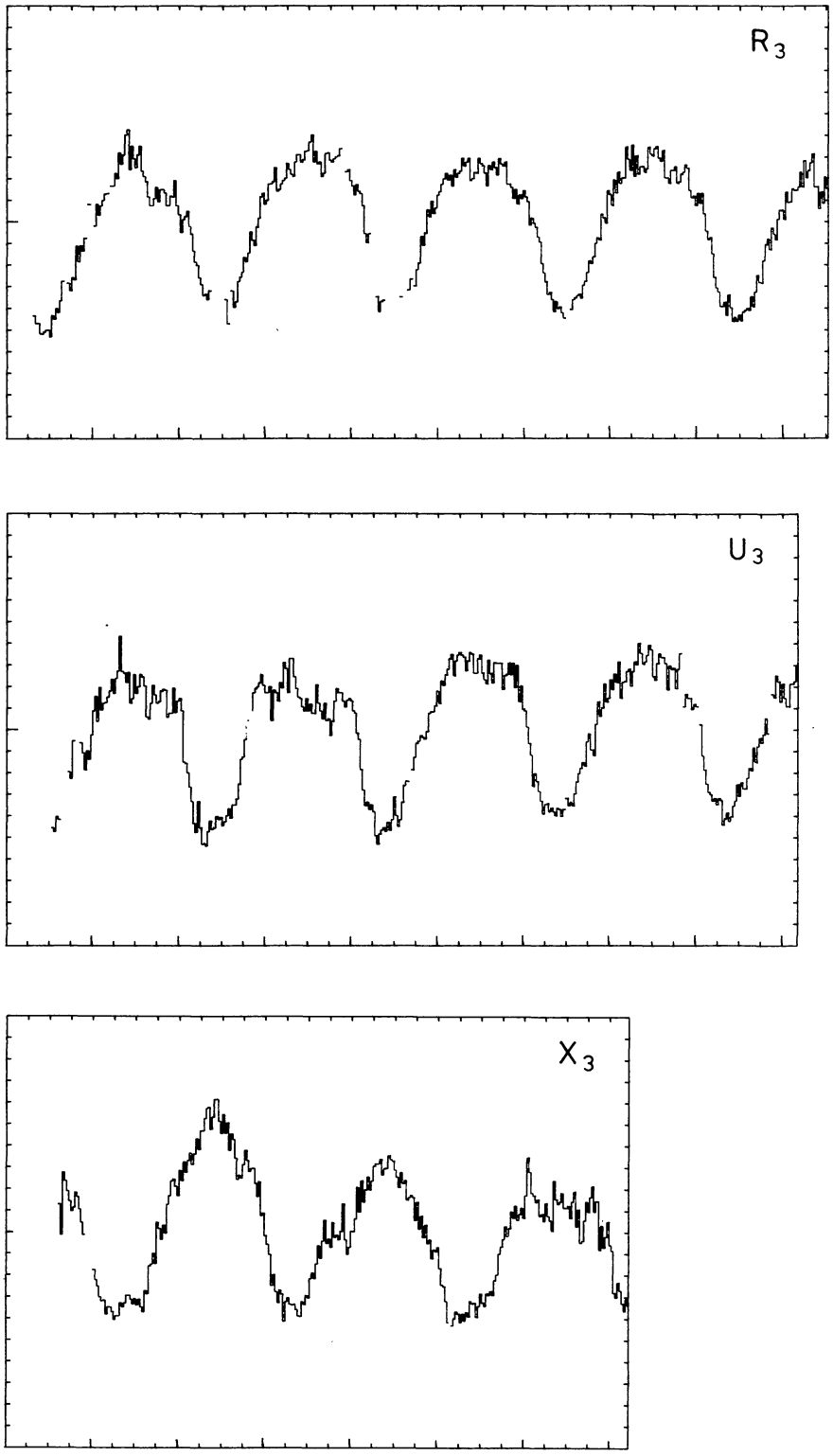

FIGURE 2*d*

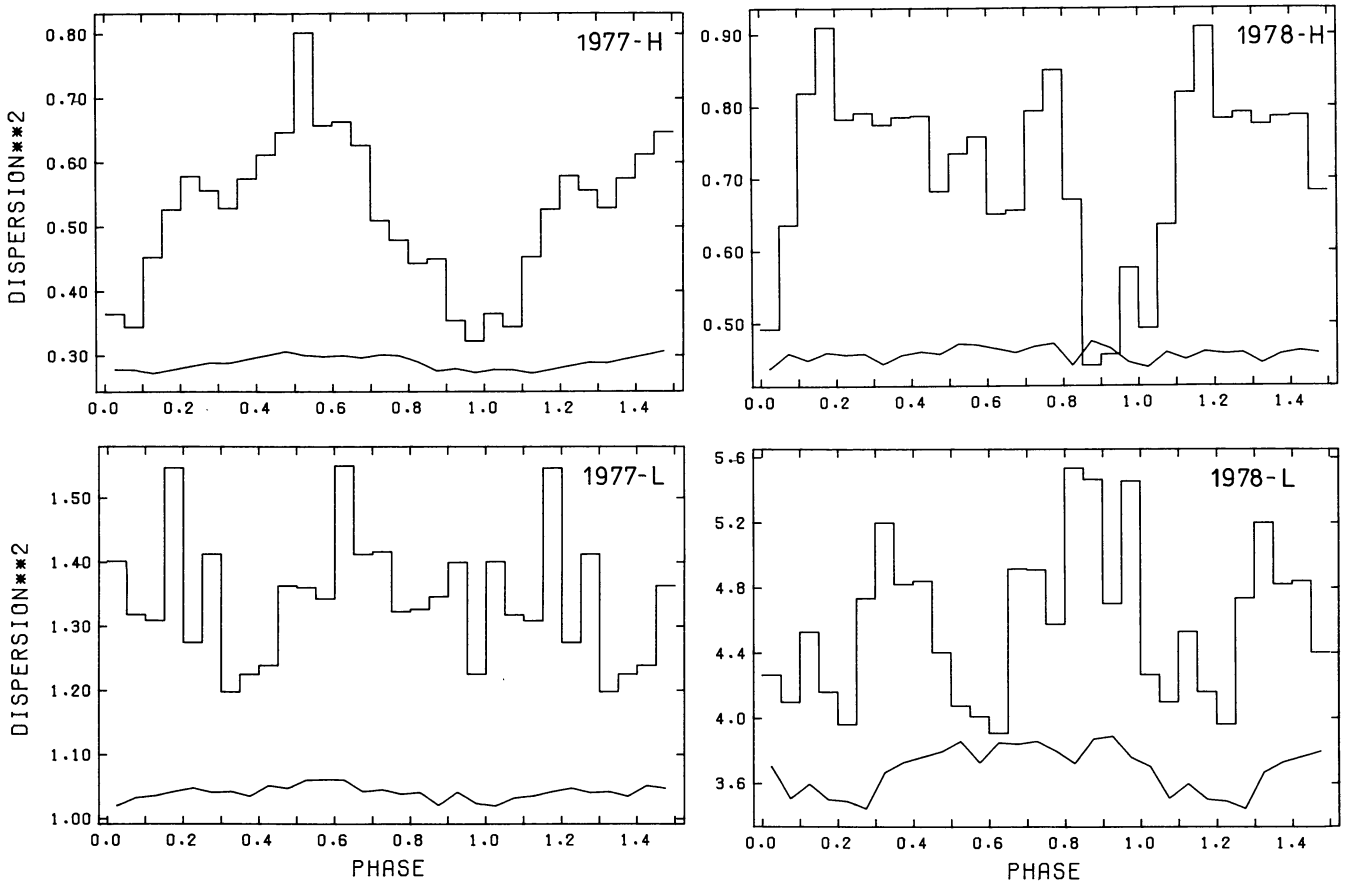

FIGURE 3*a*

FIGURE 3. — Dispersion curves of normalized folded light curves (for explanation see text). The boundaries of the data segments which were used for each curve are indicated in table I. For the 1976 and 1977 data, the dispersion values were averaged into 0.05 cycle phase bins prior to plotting. Vertical scale is in units of the square of the amplitude of the modulation.

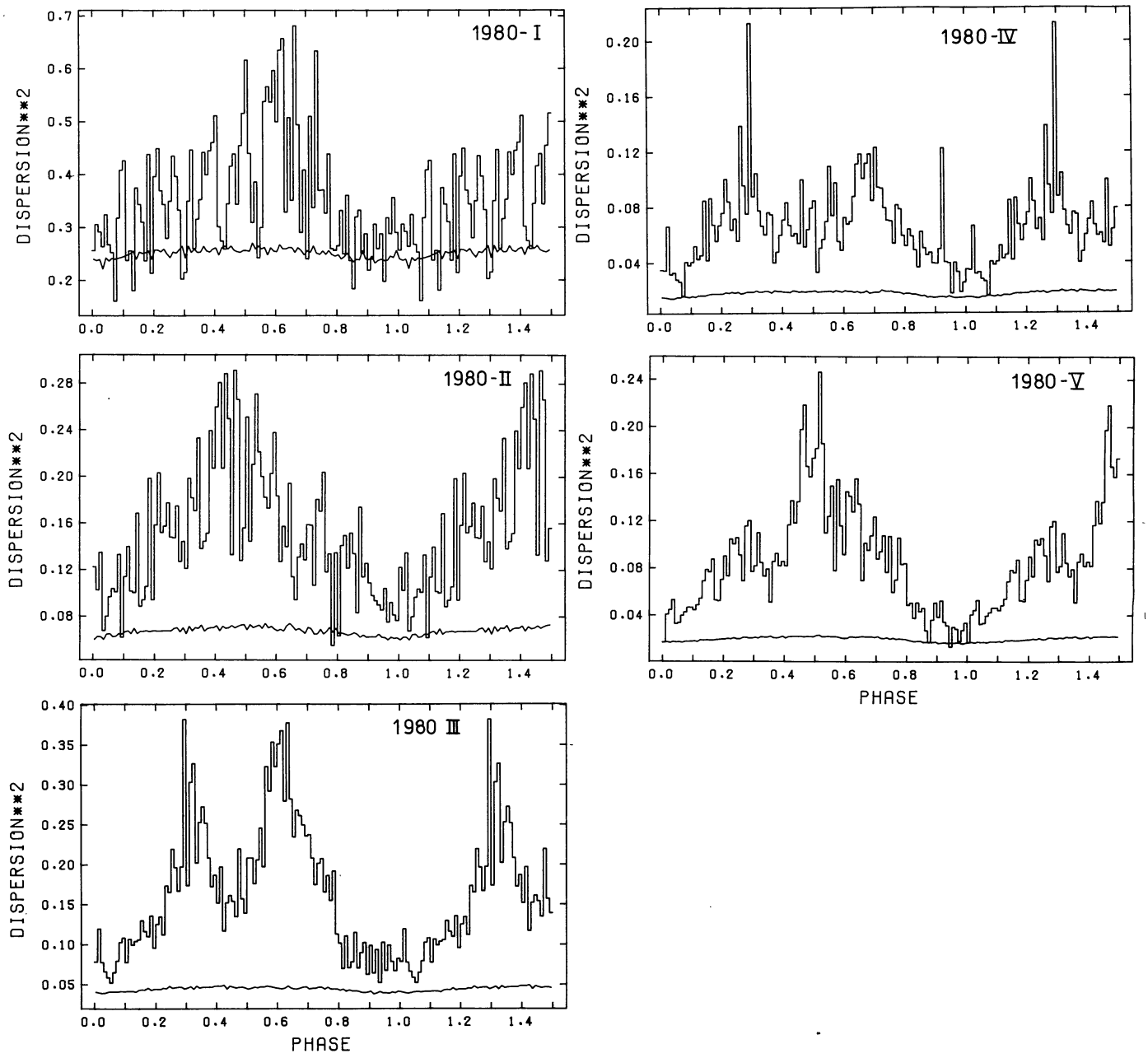

FIGURE 3*b*

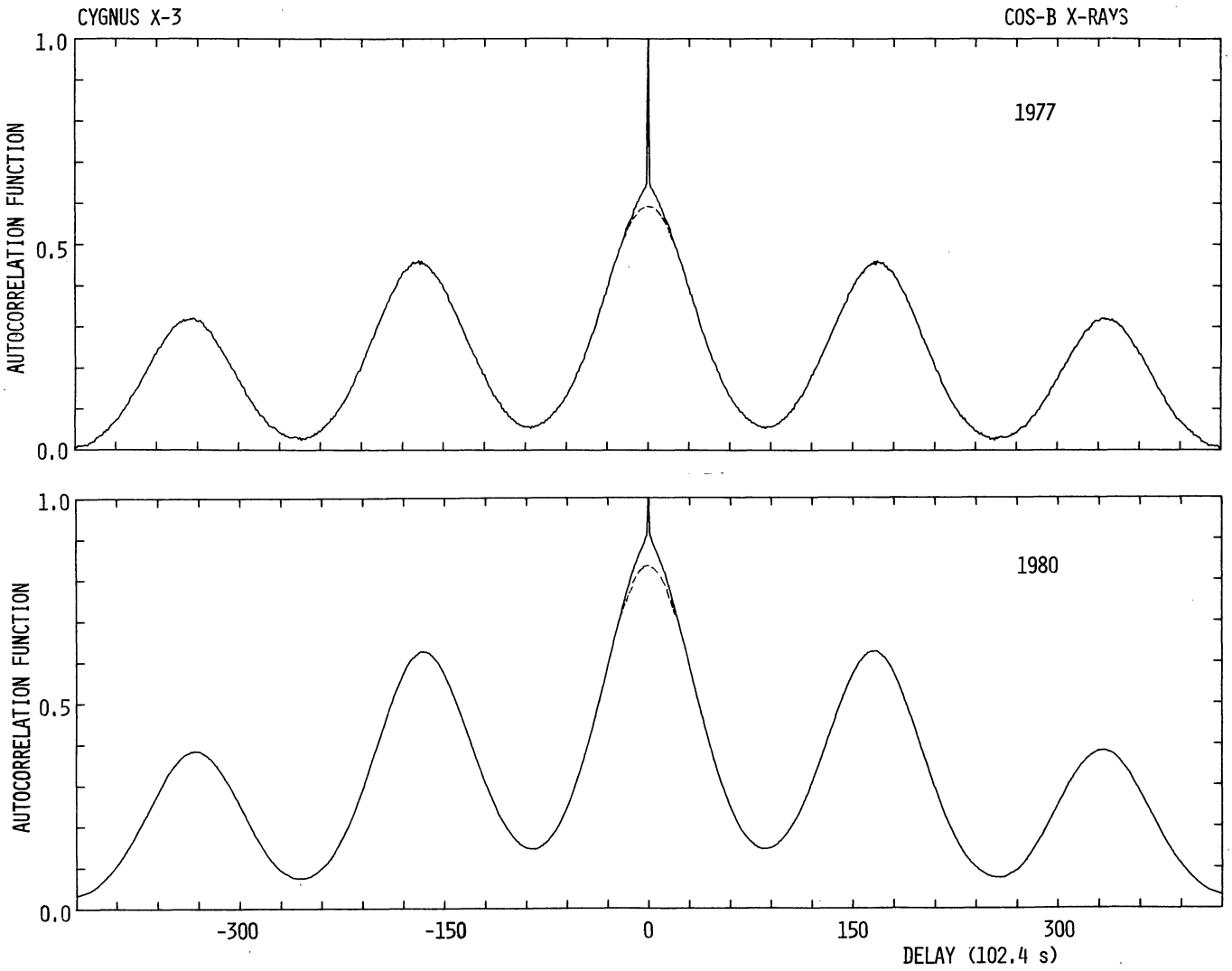

FIGURE 4. — Autocorrelation functions. The signal was normalized to a mean level of zero before calculating the autocorrelation function, utilizing FFT techniques. The general downward trend towards larger delay is an effect of the data gaps. Dashed line represents the result that would have been obtained if no short term fluctuations had occurred (excepting a sharp peak at zero delay due to statistical noise, as also visible in the actual data), as estimated from the shape of the secondary maxima (see text).